JGR Space Physics

RESEARCH ARTICLE
10.1029/2021JA029118

Whistler Wave Interactions With Superthermal Electrons on Martian Crustal Magnetic Fields: Bounce-Averaged Diffusion Coefficients and Time Scales

Alexander Shane[1] **and Michael Liemohn**[1]

[1]Department of Climate and Space Sciences and Engineering, University of Michigan, Ann Arbor, MI, USA

Key Points:

- Low-energy photoelectrons at Mars have fast wave–particle interaction time scales and can be scattered across the source cone
- High-energy photoelectrons have slow wave–particle interaction time scales which restrict scattering across the source cone
- Trapped photoelectrons energized to high energies by whistler waves can then modify the high-energy distribution

Correspondence to:
A. Shane,
adshane@umich.edu

Citation:
Shane, A., & Liemohn, M. (2021). Whistler wave interactions with superthermal electrons on Martian crustal magnetic fields: Bounce-averaged diffusion coefficients and time scales. *Journal of Geophysical Research: Space Physics*, *126*, e2021JA029118. https://doi.org/10.1029/2021JA029118

Received 11 JAN 2021
Accepted 9 MAY 2021

Abstract Pitch angle distributions of high-energy superthermal electrons (> 100 eV) observed at Mars show evidence of a ubiquitous energization process occurring on dayside crustal magnetic fields. Wave–particle interactions have been put forth as one explanation and in this study we investigate if the conditions are right at Mars for this process to occur regularly. The resonant energy of electrons is dependent on not only the whistler wave frequency and normal angle but also the characteristic energy of the plasma environment. The characteristic energy is determined by the magnetic field strength and thermal electron density, both measured quantities by the Mars Atmosphere and Volatile EvolutioN mission. Bounce-averaged diffusion coefficients are calculated using a typical characteristic energy profile and observed wave parameters. Time constants are also calculated and it is shown that wave–particle interactions are more efficient than Coulomb collisions. Low-energy electrons have fast wave–particle interaction time scales and electrons can be scattered across the source cone and energized. High-energy electrons have slow wave–particle interactions time scales and electrons energized to these energies will become trapped and modify the pitch angle distribution. Modeling the evolution of the electron distribution function will provide more insight into the process.

1. Introduction

Mars has a unique space environment relative to other planets in our solar system. The Interplanetary Magnetic Field's interaction with the ionosphere of Mars sets up an induced magnetosphere, further complicated by the presence of localized crustal fields that rotate with the planet. Superthermal electrons, electrons with energies ranging from 1 to 1,000 eV, populate these crustal field lines during their time in the dayside hemisphere. These electrons primarily consist of photoelectrons, produced from photoionization of atmospheric neutrals, with peak production occurring around 130 km. Below the photoelectron exobase, found to be ~150 km by S. Xu et al. (2016), collisions dominate and the electrons are lost locally. Above the photoelectron exobase, the particles are magnetized and can travel to high altitudes, eventually reaching the conjugate foot point of the crustal magnetic field. The magnetic field strength decreases with altitude and the electron's pitch angle becomes more field aligned as it travels to higher altitudes due to the conservation of the first adiabatic invariant. This source cone distribution is more pronounced for higher energy electrons as Coulomb collisions are proportional to $1/E^2$, where E is the energy of the electron. Figure, 1 of Shane et al. (2019) details this pitch angle distribution (PAD) evolution along a field line as a function of energy.

Data from Mars Global Surveyor (MGS) and the Mars Atmosphere and Volatile EvolutioN (MAVEN; Jakosky et al., 2015) mission have shown that our assumptions of the PADs of superthermal electrons on the Martian crustal fields are incorrect and that more physics are involved than just collisions and single particle motion. Liemohn et al. (2003) looked at a case study between MGS data and modeled electron fluxes and found that MGS measured isotropic distributions for electrons with energies greater than 100 eV. Brain et al. (2007) looked at the PADs of 115 eV electrons measured with MGS and showed that isotropic and two-sided loss cones are the most common distributions on closed crustal field lines. Shane et al. (2019) performed a statistical study using MAVEN data of superthermal electron PADs on closed crustal field lines. They showed that electrons with energies less than 60 eV have PADs that are in agreement with modeling results and that adiabatic invariants and collisions describe the evolution of their distribution. Electrons with energies greater than 60 eV were not in agreement and electrons with energies between 100 and 500 eV

had a flux peak at perpendicular pitch angles. These results were 2-year averages and indicate that unstudied physics is occurring ubiquitously on crustal fields.

Multiple explanations, including a magnetosheath source, were considered by Shane et al. (2019) and whistler mode waves were given as a probable mechanism for this flux peak at high energies as their interaction with electrons is energy dependent. Whistler waves are electromagnetic waves with frequencies between the lower hybrid frequency and the electron gyrofrequency. These waves are generated from a temperature anisotropy ($T_{e,\perp} > T_{e,\parallel}$), where $T_{e,\perp}$ and $T_{e,\parallel}$ are the perpendicular and parallel electron temperature, respectively, which was observed by Harada et al. (2016). They also saw most of their dayside wave events near the Magnetic Pileup Boundary, indicating that the waves or anisotropic electrons originated in the magnetosheath. Fowler et al. (2018) observed whistler wave generation as a byproduct of a magnetosonic wave event. The magnetosonic wave compresses the plasma, leading to a temperature anisotropy and wave growth. Fowler et al. (2020) looked at the same event but examined the effects of the whistler wave in greater detail. The waves were able to pitch angle scatter electrons, breaking their adiabaticity, and lead to parallel heating.

Quasi-linear theory is one method of analyzing wave–particle interactions which takes the Vlasov equation and separates variables into an average state and fluctuating state due to waves. This formulation of describing wave–particle interactions allows a presupposition of the wave variables (frequency and wave normal angle) and details the interaction with electrons using diffusion coefficients. Kennel and Engelmann (1966) gave the derivation of the quasi-linear diffusion equation and Lyons (1974a) transformed it into spherical coordinates (i.e., velocity and pitch angle). Lyons (1974b) then derived analytical expressions for whistler wave and ion cyclotron wave diffusion coefficients in an electron–proton plasma. More recently, Jordanova et al. (1996) investigated the effects of heavy ions on the diffusion coefficients.

In this study, we will characterize the background plasma conditions of the Mars environment using MAVEN measurements. The magnetic field strength and thermal electron density impact the energy of electrons resonant with a given whistler wave. We will use quasi-linear theory to calculate both local and bounce-averaged diffusion coefficients for Mars crustal field conditions. Few measurements of whistler waves have been observed at Mars, but we will use the observed wave parameters as inputs into our bounce-averaged calculations. Time constants of the wave–particle interaction will be calculated to estimate the efficiency of the interaction and compared to other relevant time scales such as the bounce period and Coulomb collision time constants.

2. Diffusion Coefficient Calculations

In this section, we will describe the main equations and steps used to calculate the diffusion coefficients described by quasi-linear theory. The full details of the calculation and complete equation sets can be found in Lyons (1974b) and Jordanova et al. (1996). We note that these equations are nonrelativistic and relativistic formulations can be found in Glauert and Horne (2005) and Albert (2005). Throughout this paper, we will be including the heavy ion effects from Jordanova et al. (1996). We will assume for this study that the ion composition of the upper Martian ionosphere contains 66% O^+ and 34% O_2^+, corresponding to altitudes > 300 km.

2.1. Resonant and Characteristic Energies

The resonance condition for wave–particle interactions is given in Equation 1 where $v_\parallel$ is the parallel velocity of the particle relative to the local magnetic field, ω_k is the wave frequency as a function of the wave vector $\mathbf{k}$, $\Omega = qB/m$ is the particle's cyclotron frequency, q is the particle's charge, B is the magnetic field strength, m is the particle's mass, and n is the harmonic, with Landau resonance given by $n = 0$:

$$v_\parallel = \frac{\omega_k}{k_\parallel} - \frac{n\Omega}{k_\parallel} \tag{1}$$

This equation states that the parallel velocity of the particle relative to the local magnetic field is equal to the parallel phase velocity of the wave. For harmonics $|n| > 0$, the wave frequency as seen by the particle

is Doppler shifted by its parallel motion. Considering electrons as the resonant particle, waves where $(\omega_{pe} / \Omega_e)^2 \gg \omega / \Omega_e$, the resonance condition (Equation 1), and the dispersion relation described by cold plasma theory (Equation 7 in Lyons [1974b]), the parallel kinetic energy of particles resonant with whistler waves can be calculated using Equation 2:

$$E_{\parallel,\mathrm{res}} = E_c \frac{\left(1 + n\Omega_e / \omega_k\right)^2}{\cos^2\theta} \Psi \tag{2}$$

$$E_c = \frac{B^2}{2\mu_0 n_e} \tag{3}$$

Here, Ω_e no longer contains the sign of the charge (as well as for the remainder of this paper), and θ is the wave normal angle (the angle between the wave vector and the magnetic field). Ψ is a function of the wave normal angle and normalized wave frequency (ω_k/Ω). In the presence of heavy ions, Ψ is also a function of the fractional densities, mass ratios, and charge numbers of each ion species (for brevity, we point the reader to Equations 8–12 in Jordanova et al. [1996]). The characteristic energy E_c, or available magnetic energy per particle, is given in Equation 3 and is strictly a function of the background magnetic field strength B and thermal electron density n_e. This means that the energy of electrons resonant with a given whistler wave is dependent on the ambient plasma conditions.

2.2. Diffusion Coefficients

The quasi-linear diffusion equation as given by Lyons (1974a) is

$$\frac{\partial f}{\partial t} = \frac{1}{v \sin\alpha} \frac{\partial}{\partial \alpha} \left\{ \sin\alpha \left(D_{\alpha\alpha} \frac{1}{v} \frac{\partial f}{\partial \alpha} + D_{\alpha v} \frac{\partial f}{\partial v} \right) \right\} + \frac{1}{v^2} \frac{\partial}{\partial v} \left\{ v^2 \left(D_{v\alpha} \frac{1}{v} \frac{df}{d\alpha} + D_{vv} \frac{\partial f}{\partial v} \right) \right\} \tag{4}$$

where f is the electron distribution function, α and v are the electron's pitch angle and velocity, respectively, and the pitch angle, mixed, and velocity diffusion coefficients ($D_{\alpha\alpha}$, $D_{\alpha v}$, D_{vv}) are given in 5:

$$\begin{aligned} D_{\alpha\alpha} &= \sum_{n=-\infty}^{\infty} \int_0^{x_{\max}} x\, D_{\alpha\alpha}^{nx}\, dx \\ D_{\alpha v} = D_{v\alpha} &= \sum_{n=-\infty}^{\infty} \int_0^{x_{\max}} x\, D_{\alpha v}^{nx}\, dx \\ D_{vv} &= \sum_{n=-\infty}^{\infty} \int_0^{x_{\max}} x\, D_{vv}^{nx}\, dx \end{aligned} \tag{5}$$

The diffusion coefficients need to be calculated as a function of harmonic n and wave normal angle θ. They are then summed over each harmonic and integrated over $x = \tan(\theta)$. In reality, only the pitch angle term needs to be calculated as the mixed and velocity terms are related by

$$\begin{aligned} D_{\alpha v}^{nx} &= D_{\alpha\alpha}^{nx} \left[\frac{\sin\alpha\cos\alpha}{-\sin^2\alpha - n\Omega / \omega_k} \right] \Bigg|_{\omega_k/\Omega = (\omega_k/\Omega)_{\mathrm{res}}} \\ D_{vv}^{nx} &= D_{\alpha\alpha}^{nx} \left[\frac{\sin\alpha\cos\alpha}{-\sin^2\alpha - n\Omega / \omega_k} \right]^2 \Bigg|_{\omega_k/\Omega = (\omega_k/\Omega)_{\mathrm{res}}} \end{aligned} \tag{6}$$

In order to calculate the diffusion coefficients, the frequency and wave normal angle distribution of the whistler waves must be specified. We use Gaussian distributions in both frequency and x to describe such distributions in this study (Equations 7 and 8, respectively).

$$B^2(\omega) = \begin{cases} B_0^2 \exp\left(-\left(\dfrac{\omega - \omega_m}{\delta\omega}\right)^2\right) & \omega_{lc} \le \omega \le \omega_{uc} \\ 0 & \text{otherwise} \end{cases} \tag{7}$$

$$g(x) \propto \begin{cases} \exp\left(-\left(\dfrac{x - x_m}{\delta x}\right)^2\right) & x_{lc} \le x \le x_{uc} \\ 0 & \text{otherwise} \end{cases} \tag{8}$$

The variables needed to describe these distributions are the peaks (ω_m, x_m), the half widths ($\delta\omega$, δx), the upper and lower cutoffs where waves do not exist outside of the given range (ω_{lc}, ω_{uc}, x_{lc}, x_{uc}), and the wave energy density, B_0^2. These distributions can be easily changed if observations indicate that these variables are not normally distributed. The final equation for the diffusion coefficient is as follows:

$$D_{\alpha\alpha}^{nx} = |\Omega| \frac{|B_{wave}^2}{B^2} v^2 \sqrt{\pi} \frac{\cos^5\theta \left(\dfrac{\Omega}{\delta\omega}\right)\left(-\sin^2\alpha - \dfrac{n\Omega}{\omega_k}\right)^2}{\sqrt{\Psi^3}\ |1 + \dfrac{n\Omega}{\omega_k}|^3\ I(\omega_k)} |\Theta_{n,k}|^2 \frac{\exp\left[-\dfrac{(\omega_k - \omega_m)^2}{\delta\omega^2} - \dfrac{(x - x_m)^2}{\delta x^2}\right]}{\operatorname{erf}\left[\dfrac{\omega_{uc} - \omega_m}{\delta\omega}\right] + \operatorname{erf}\left[\dfrac{\omega_m - \omega_{lc}}{\delta\omega}\right]} \left(1 - \frac{1}{v_{||}} \frac{\delta\omega_k}{\delta k_{||}}\ |_x\right)^{-1} \Bigg|_{\omega_k/\Omega = (\omega_k/\Omega)_{\text{res}}} \tag{9}$$

In Equation 9, B_{wave}^2 is the total wave amplitude and can be computed from Equation 7. $|\Theta_{n,k}|$, $I(\omega_k)$, and $\left(1 - \frac{1}{v_{||}} \frac{\delta\omega_k}{\delta k_{||}}\right)$ are all functions of the wave parameters and the latter two are modified by the presence of heavy ions. We point the reader to Lyons (1974b) and Jordanova et al. (1996) for full details on this derivation. In order to calculate the diffusion coefficients as a function of energy and pitch angle for a given whistler wave distribution (number of harmonics, frequency, wave normal angle, and B_{wave}), the steps are as follows:

1. Calculate the characteristic energy (E_c) from the magnetic field strength and thermal electron density.
2. For each harmonic/wave normal angle combination, determine the parallel resonant energies as a function of wave frequency (Equation 2).
3. For each energy, determine which pitch angles the parallel resonant energies correspond to.
4. Calculate diffusion coefficients for each resonant frequency as a function of pitch angle, wave normal angle, and harmonic.
5. Integrate over wave normal angle range.
6. Sum over specified harmonics.

The resultant diffusion coefficient distribution in energy–pitch angle space have units of $cm^2\ s^{-3}$. However, these are local coefficients and bounce-averaged diffusion coefficients give a more complete description of the wave–particle interaction as an electron travels along a field line.

2.3. Bounce Averaging

The local diffusion coefficients only give information about the wave–particle interaction at a single location, but the electrons and the wave are traveling along the magnetic field line. The energy and local pitch angle of an electron dictate how fast it travels through any given region, and the pitch angle changes with varying magnetic field strength. The characteristic energy and normalized wave frequency will also change, shifting the diffusion coefficient distribution in energy–local pitch angle space. Bounce-averaged diffusion coefficients take into account these changes and provide an aggregate description of the wave–particle

interaction (e.g., Lyons et al., 1972; Zhao et al., 2015). The equations are given in Equation 10, where α_{eq} is the equatorial pitch angle of the electron and the superscript *ba* denotes bounce averaged. τ_b is the bounce period of an electron and is given in Equation 11. Here, we are assuming a symmetric dipole field line where s_1 and s_2 are the mirror point and top of the field line, respectively. The integral is over a quarter-bounce and therefore a factor of 4 is needed.

$$\begin{aligned} D_{\alpha\alpha}^{ba}(E,\alpha_{eq}) &= \frac{4}{\tau_b(E,\alpha_{eq})\,v}\int_{s_1}^{s_2} D_{\alpha\alpha}(E,\alpha)\left(\frac{\partial\alpha_{eq}}{\partial\alpha}\right)^2\frac{ds}{\cos\alpha} \\ D_{EE}^{ba}(E,\alpha_{eq}) &= \frac{4}{\tau_b(E,\alpha_{eq})\,v}\int_{s_1}^{s_2} D_{EE}(E,\alpha)\,\frac{ds}{\cos\alpha} \end{aligned} \tag{10}$$

$$\tau_b(E,\alpha_{eq}) = \frac{4}{v}\int_{s_1}^{s_2}\frac{ds}{\cos\alpha} \tag{11}$$

3. Characteristic Energies Observed by MAVEN

The resonant energy and pitch angle of superthermal electrons with a given wave are determined by the frequency and wave normal angle of the wave. The characteristic energy is a multiplicative scaling factor determined by the local magnetic field strength and thermal electron density. These are both quantities measured by MAVEN and the characteristic energy distribution of the Martian space environment can be quantified and used to construct representative altitude profiles for calculating bounce-averaged diffusion coefficients.

We use data from the Magnetometer (MAG; Connerney et al., 2015) and the Langmuir Probes and Waves (LPW; Andersson et al., 2015) instruments to analyze the characteristic energies observed in the Martian space environment. We use the same criteria as Shane et al. (2019) to filter for dayside crustal fields for continuity between the PADs and the characteristic energies measured. The solar zenith angle must be less than 90° to ensure dayside observations. All observations are at altitudes greater than 200 km so that our measurement is above the photoelectron exobase and the electrons are magnetized. The shape parameter (S. Xu et al., 2017) is used to determine that photoelectrons are in the source cone. This looks at the energy spectrum of 20–80 eV electrons at field-aligned pitch angles and determines a goodness of fit to a typical photoelectron spectra. A magnetic field minimum of 20 nT is used so that we exclude deeply draped fields and a spacecraft potential filter is also set.

Figure 1 plots the combined 2D histogram of magnetic field strength and thermal electron density observed with MAVEN on dayside crustal fields. The histograms for each individual quantity are plotted on the right and top left subplots. We mask any bin with sample size < 10 and the maximum sample size in a bin is 2,500. Overlaid on the 2D histogram are characteristic energy contours. In the upper right of the figure is a histogram of all characteristic energies observed. This value spans orders of magnitude with the majority of observations between $E_c = 0.1$ and 100 eV. Some studies use the value $f_{pe}/f_{ce} = (E_c\ /\ m_e c^2)^{-\frac{1}{2}}$, the ratio of the plasma to electron cyclotron frequency, instead. Characteristic energies of 0.1, 1, 100, and 1,000 eV correspond to f_{pe}/f_{ce} = 2,262.3, 715.4, 226.2, and 71.5, respectively.

Figure 2 further explores the characteristic energy distribution at Mars by plotting the median value against (a) altitude, (b) local time, and (c) magnetic elevation angle. The magnetic elevation angle is defined to be 0° when parallel with the surface and 90° when perpendicular. The region between the 25th and 75th percentiles is shaded. The geometric mean lies on top of the median and the arithmetic mean is much greater than the 75th percentile, highlighting the lognormal distribution of the characteristic energy. The altitude profile shows that the characteristic energy is likely to be greater at higher altitudes. While both the magnetic field and electron density typically decrease with altitude, the electron density can vary over orders of magnitude, dominating the net change to the characteristic energy. There is little-to-no dependence on local time and magnetic elevation angle. However, the characteristic energy on horizontal field lines has a longer tail to the distribution.

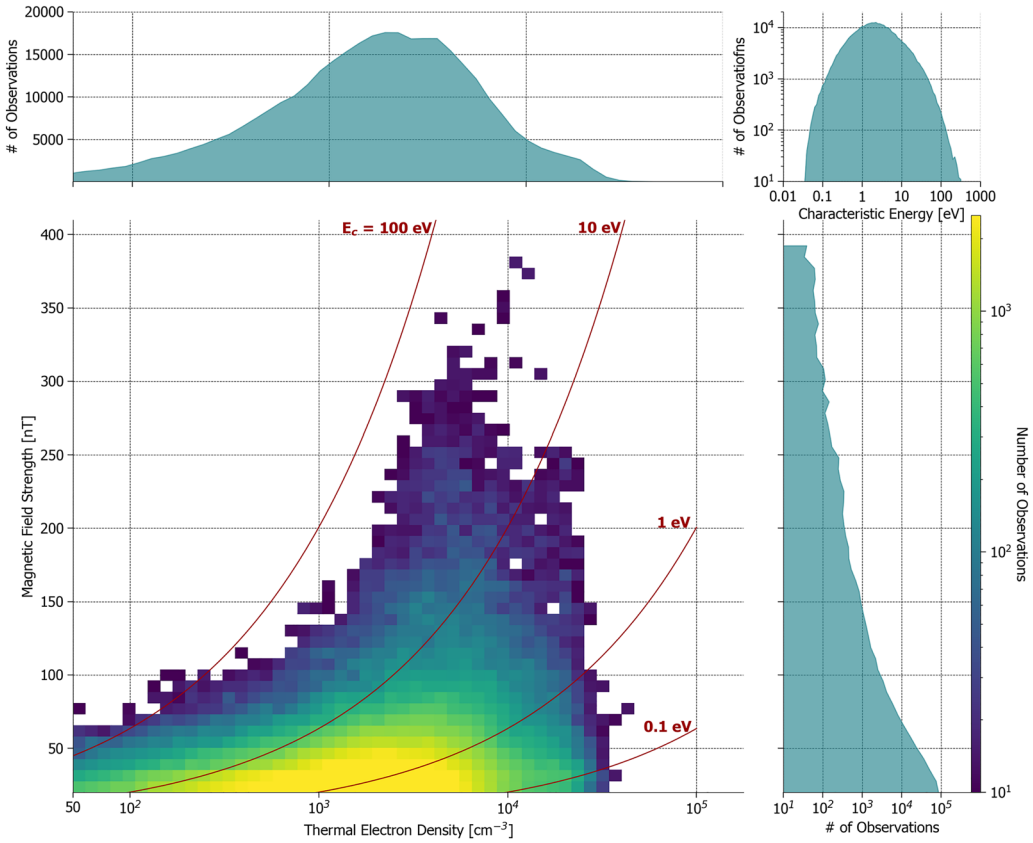

Figure 1. Histograms of the magnetic field strength and thermal electron density observed on dayside closed crustal fields at Mars. The color scale is logarithmic and ranges from 10 to 2,500 observations. Bins with sample size <10 are not colored. Characteristic energy contours are shown in red. Histogram of the characteristic energy is shown in the upper right.

4. Local Diffusion Coefficients Distribution

In Figure 3, we show local pitch angle (top row) and energy (bottom row) diffusion coefficient distributions for two characteristic energies: 30 eV (left column) and 100 eV (right column). The whistlers observed by Harada et al. (2016) were on the order of $0.1\Omega_e$ propagating quasi-parallel to the magnetic field. Those observed by Fowler et al. (2020) were between 0.1 and $0.5\Omega_e$ and while they could not estimate the wave

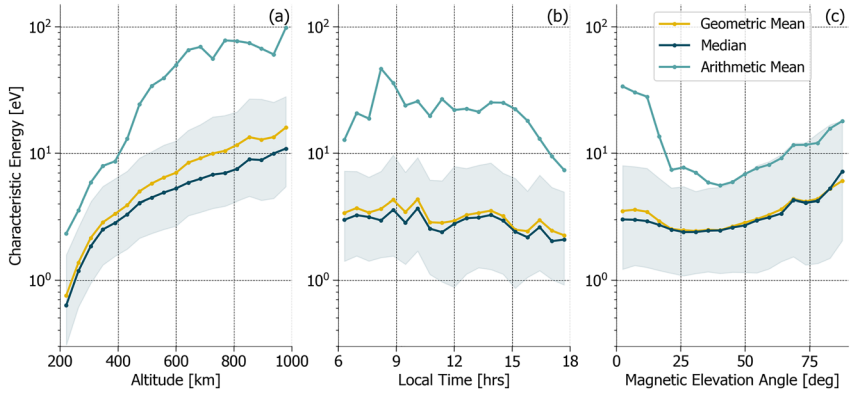

Figure 2. Characteristic energy distribution as a function of (a) altitude, (b) local time, and (c) magnetic elevation angle. The geometric mean, arithmetic mean, and median are all plotted and the region between the 25th and 75th percentiles is shaded.

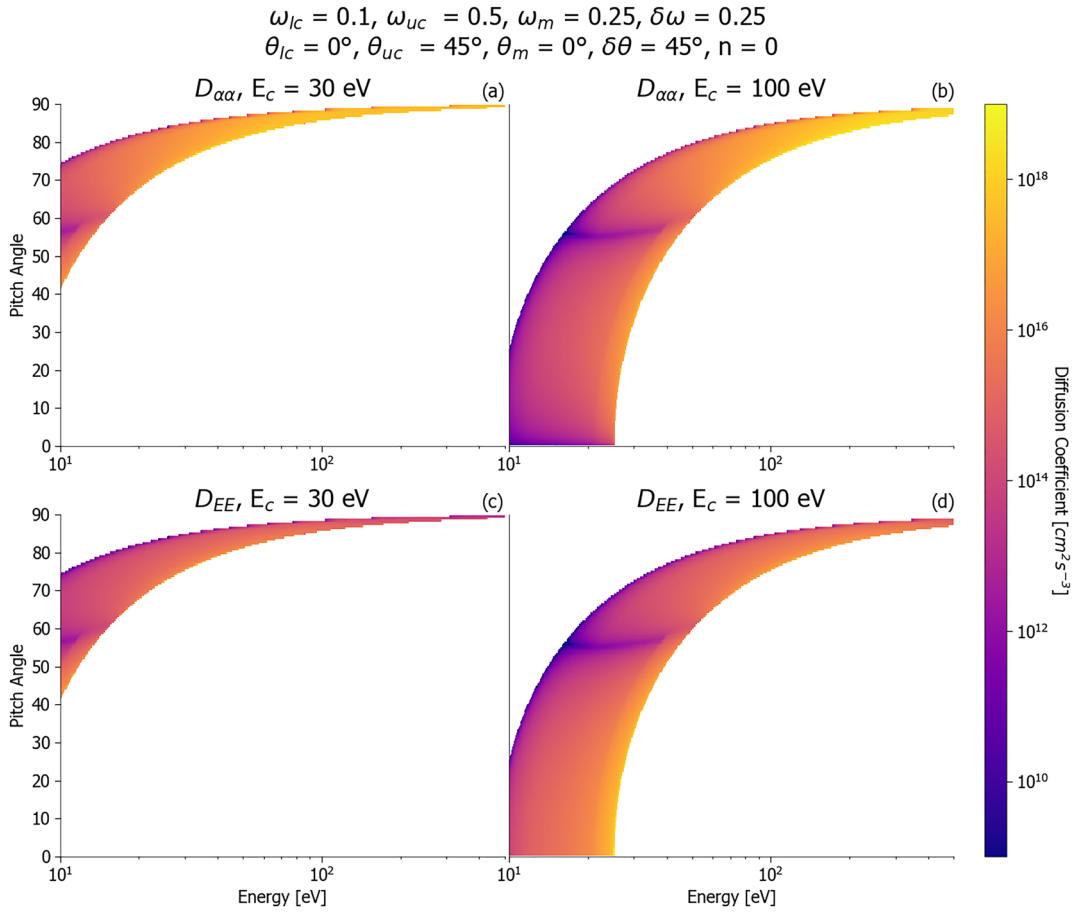

Figure 3. Pitch angle (top) and energy (bottom) diffusion coefficients for two characteristic energies: 30 eV (left) and 100 eV (right). The color scale is logarithmic and ranges 9 orders of magnitude. White regions indicate that no wave–particle interaction occurs at that location in velocity space.

normal angle, at these frequencies the resonance cone limits wave propagation at angles higher than ~60°. In this study, we will use a wave frequency distribution that ranges from $\omega_{lc} = 0.1\Omega_e$ to $\omega_{uc} = 0.5\Omega_e$, with the peak at $\omega_m = 0.25\Omega_e$ and the width $\delta\omega = 0.25\Omega_e$. The wave normal angle distribution is assumed to be quasi-parallel from $\theta_{lc} = 0°$ to $\theta_{uc} = 45°$, peaked at $\theta_m = 0°$ and width $\delta\theta = 45°$. The value of the wave energy density, B_0^2, is taken from Harada et al. (2016). The values observed in their study were between 10^{-4} and 10^{-2} nT^2/Hz and we use a conservative low value of 10^{-4} nT^2/Hz here. Only Landau resonance ($n = 0$) is shown in Figure 3. The shape of these distributions traces the curve defined by $E_{res} = E_{\parallel,res}/\cos^2(\alpha)$ and the white space denotes areas where wave–particle interactions do not occur for the specified wave in the chosen characteristic energy environment. For harmonics $|n| \geq 0$, the diffusion coefficient distribution will be a superposition of each harmonic resonant energy curve.

Other wave parameters were investigated and results are described here. An increase to the characteristic energy shifts the entire diffusion coefficient distribution to higher energies, while a decrease in characteristic energy shifts the distribution to lower energies. Decreasing the width of the Gaussian in frequency to $\delta\omega = 0.1\Omega_e$ decreases the magnitude of the diffusion coefficients for all energies and pitch angles and increasing the width to $\delta\omega = 0.5\Omega_e$ increases the magnitude of the diffusion coefficients. Shifting the peak of the wave frequency Gaussian puts more wave power into those frequencies near the peak. A shift of the peak to the lower cutoff frequency increases the magnitude of the diffusion coefficients of those electrons resonant with the lower frequencies, that is, the lower energy resonant curves of the diffusion coefficient distribution. The diffusion coefficients along the higher energy resonant curves are decreased. The opposite is true if the frequency peak is moved to the upper cutoff frequency. In this case, the magnitudes of the

diffusion coefficients are increased along the higher energy resonant curves and the diffusion coefficients along the lower energy resonant curves are decreased. Quantifying the exact energies of the resonant curves which see an increase or decrease to the diffusion coefficients along them is determined by where the two Gaussians in resonant frequency intersect. The combination of $\frac{\Psi}{\cos^2\theta}$ in Equation 2 results in field-aligned whistler waves contributing to the entire diffusion coefficient distribution. The more oblique the wave normal angle is the less it contributes to the lower energy resonant curves. Therefore, shifting the peak of the Gaussian in wave normal angle to more oblique wave normal angles increases the magnitude of the diffusion coefficients along higher energy resonant curves and decreases the magnitude along the lower energy curves. Halving the Gaussian width in wave normal angle puts less wave power into more oblique waves and therefore this has the opposite effect as shifting the peak. The changes made to the Gaussian parameters in frequency and wave normal angle only have the effect of altering along which corresponding $E_{\parallel,\mathrm{res}}$ curves will have a higher or lower diffusion coefficient magnitude. As long as the upper and lower cutoffs are held constant, the shape and area of the diffusion coefficient distribution will also remain constant.

5. Bounce-Averaged Diffusion Coefficients

The motion of both electrons and the whistler wave along the field line makes interpretation of local diffusion coefficients limited. Bounce averaging takes into account the change in pitch angle of the electron, the time the electron spends in any given region along the magnetic field, the local characteristic energy, and the change in normalized wave frequency as the local gyrofrequency is shifted due to the change in magnetic field strength. In this section, we perform three runs of an idealized bounce-averaging model on a Martian crustal field line. The three runs differ by the characteristic energy profile used along the field line.

5.1. Methodology

Some background parameters for our bounce-averaged runs are shown in Figure 4. Using the dipole field equations, we set up an idealized crustal field. Given a minimum and maximum magnetic field strength and the vertical distance between the two values, a dipole field can be constructed. The field extends from the exobase at 160 km where the field strength is ~294 nT to the top of the crustal field at 500 km with a field strength of 50 nT. A thermal electron density profile is taken from MGITM (Bougher et al., 2015) and the log of the density is linearly interpolated above 250 km. For Run 1, we increase the thermal electron density profile by a factor of 5 to reproduce the geometric mean/median characteristic energy distribution observed by MAVEN. No change is made for Run 2 and the resulting characteristic energy distribution is representative of the arithmetic mean measured by MAVEN. For direct comparison, these MAVEN profiles are plotted again in Figure 4. Lastly, we divide the electron density profile by a factor of 5 for Run 3. This is to investigate the wave–particle interactions at high characteristic energies, which causes less interaction with low-energy electrons. Above 300 km, we use the rough assumption that the ion composition consists of 66% O^+ and 34% O_2^+, and for altitudes below 300 km the ion composition is made up of 90% O_2^+ and 10% CO_2^+. We note that the addition of heavy ions has little effect on the calculations because the assumed wave frequencies are much greater than the ion gyrofrequencies. The normalized frequency and wave normal angle distribution of the whistler wave are identical to those in Figure 3 and the frequency is unnormalized by the gyrofrequency at the top of the field line. The normalized frequency of the wave is then dependent on the location along the magnetic field, and the actual frequency of the wave (in Hz) remains constant. No effort is made to model the change in wave normal angle as the wave propagates and the wave is assumed to exist at all locations along the field line. For the bounce-averaged runs, we include harmonics $|n| \leq 3$, as these higher harmonics will affect the energies of interest. Although the crustal fields are not symmetric about the Martian equator, we will still use the term "equatorial pitch angle" to indicate the minimum-B pitch angle.

Care is needed around the bounce location to achieve convergence. This is accomplished by defining a refinement region where the magnetic field grid has a higher resolution. The magnetic field strengths where the electron's local pitch angle is between 89° and 90° define this region and are different depending on the equatorial pitch angle of the electron. We found that using 1,000 grid points to define the magnetic

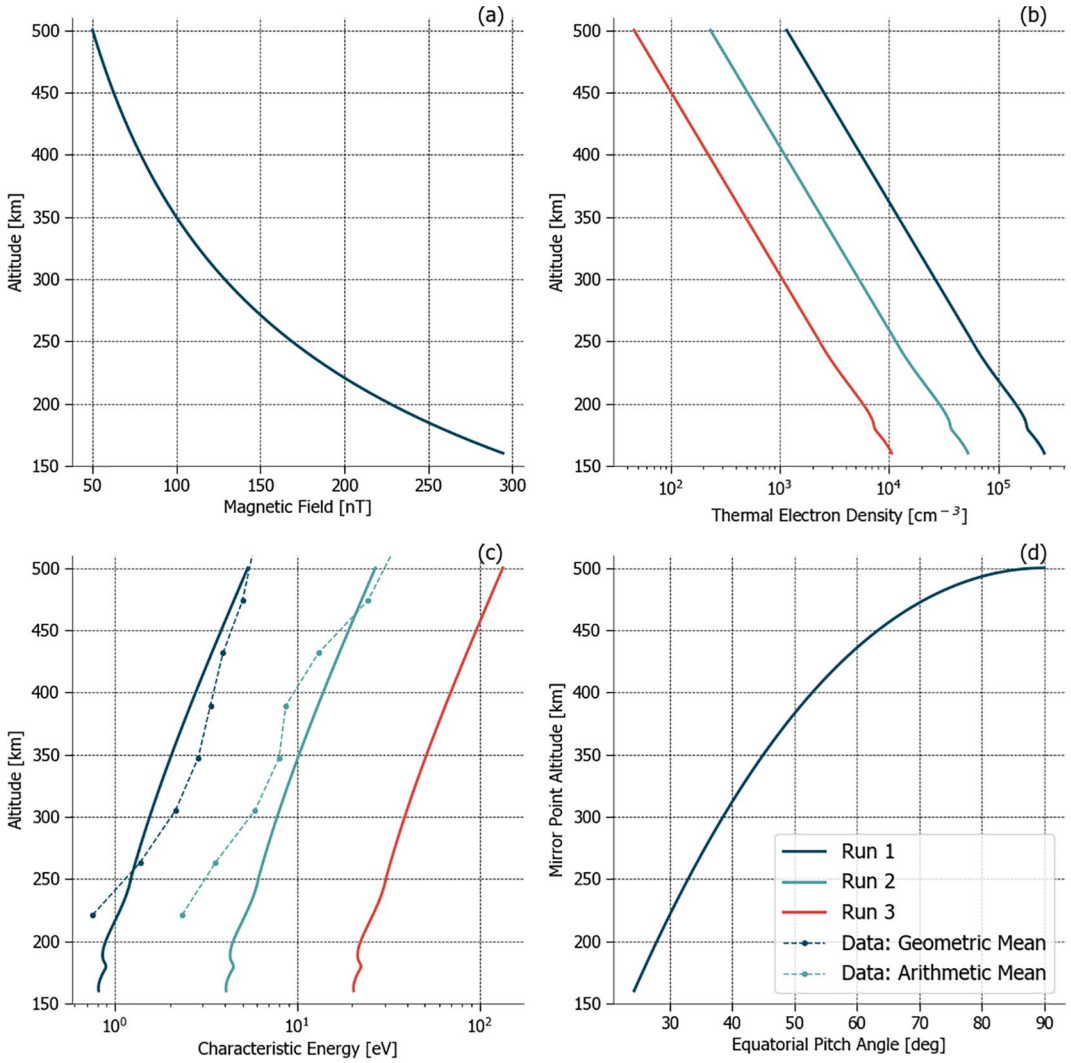

Figure 4. (a) Magnetic field strength of the dipole crustal field. (b) Electron density profiles with a factor of 5 difference between Run 2 and Runs 1 and 3. (c) Characteristic energy altitude profile for each run (solid lines) and measured by MAVEN (dashed lines). (d) Mirror point altitude of electrons with varying equatorial pitch angles. MAVEN, Mars Atmosphere and Volatile EvolutioN.

field, with a third of them used in the refinement region, is sufficient to achieve convergence of the bounce integrals.

The foot points of the dayside crustal fields are embedded in the ionosphere and so there is a constant source of electrons at field-aligned pitch angles. These electrons stream from one foot point to the other and likely deposit their energy on the conjugate side. Some of these electrons will be pitch angle scattered so their mirror point is at a higher altitude than the photoelectron exobase. We calculate bounce-averaged diffusion coefficients for both populations, the source cone and the trapped electrons. In these calculations, we assume that all source cone electrons are lost upon reaching the conjugate ionosphere, and thus the integral is only over half a bounce period. It is important to note that the source cone electrons are thought to be the main population of electrons on closed crustal fields and should be included in these calculations.

Figure 5 shows the pitch angle trajectories through altitude and local pitch angle space given multiple equatorial pitch angles. The third run conditions are used here. The color is the magnitude of the diffusion coefficients and graphically depicts where wave–particle interactions occur in altitude for 25 eV electrons. While the pitch angle trajectories are independent of energy, the diffusion coefficient distribution will vary.

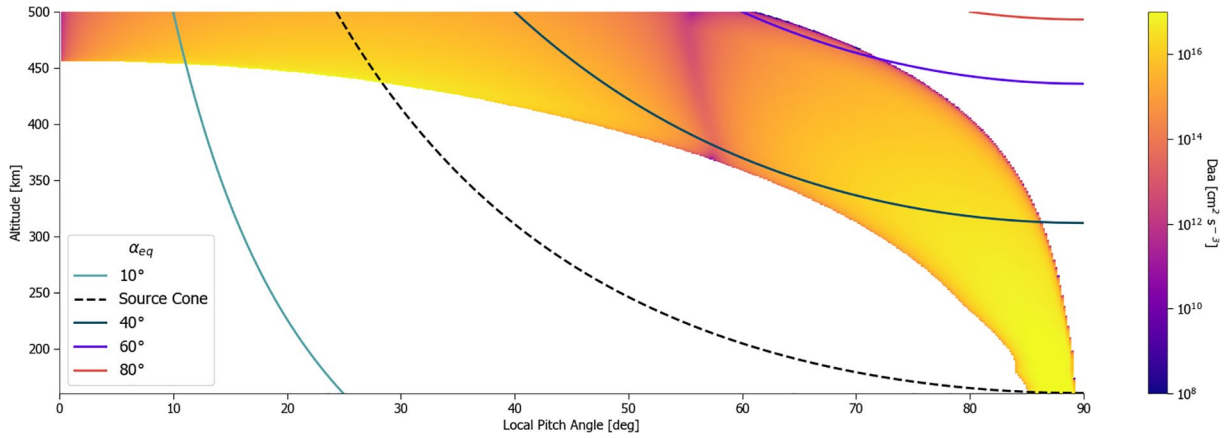

Figure 5. Trajectories of electrons with different equatorial pitch angles through altitude–pitch angle space for Run 3 conditions. The color depicts the magnitude of diffusion coefficients and maps the region where wave–particle interactions will occur with 25 eV electrons. The color scale is logarithmic and spans over 9 orders of magnitude. White regions indicate that resonance is not possible for 25 eV electrons at that local pitch angle and altitude.

A 25 eV electron with an equatorial pitch angle of 60° will have little interaction with the specified wave during its bounce period, while the 40° electron will be in resonance with the wave for the majority of its bounce. An electron on the edge of the source cone (24.33°) will not be in a wave–particle interaction region for most altitudes but is in resonance near its bounce, where the most time is spent. This figure highlights the necessity to calculate the bounce-averaged coefficients as opposed to looking at a single location along the field line.

It is useful to consider the relative importance of wave–particle interactions against other processes influencing the superthermal electron distribution on Mars crustal field lines. Above the exobase, although electrons are considered magnetized, Coulomb collisions still have an influence on the PADs, especially at lower energies. A comparison of the time scales of wave–particle interactions to the Coulomb collision time scale will provide insight into the effectiveness of the pitch angle scattering and energization of superthermal electrons due to waves. Order-of-magnitude estimates of the time constants of wave–particle interactions have been calculated as

$$\tau = \frac{v^2}{D} \tag{12}$$

which arises from dimensional analysis of Equation 4 (e.g., Liemohn et al., 1997; Lyons, 1974a). This is a rough estimate that completely ignores variations in D or f but yields an order-of-magnitude value that can be assessed for effectiveness. Coulomb collisions time scales can be calculated as

$$\tau_{cc} = \frac{\beta^4 v^3}{2\, A n_e} \tag{13}$$

where $\beta = 1.7 \times 10^{-8}\sqrt{eV}\ s\ cm^{-1}$, $A = 2.6 \times 10^{-12}\ eV^2\ cm^2$, v is the electron's velocity, and n_e is the thermal electron density (Liemohn et al., 1997). These quantities can be calculated using bounce-averaged diffusion coefficients and thermal electron density and will be compared to determine the relative effectiveness of the wave–particle interactions.

5.2. Results

Figure 6 plots the bounce-averaged diffusion coefficients for Runs 1, 2, and 3 (left, middle, and right columns, respectively). The top row plots the pitch angle diffusion coefficients and the bottom row plots the energy diffusion coefficients. The source cone pitch angle is denoted by a black dashed line. The shift of the diffusion coefficient distribution to higher energies due to the higher characteristic energy profiles used

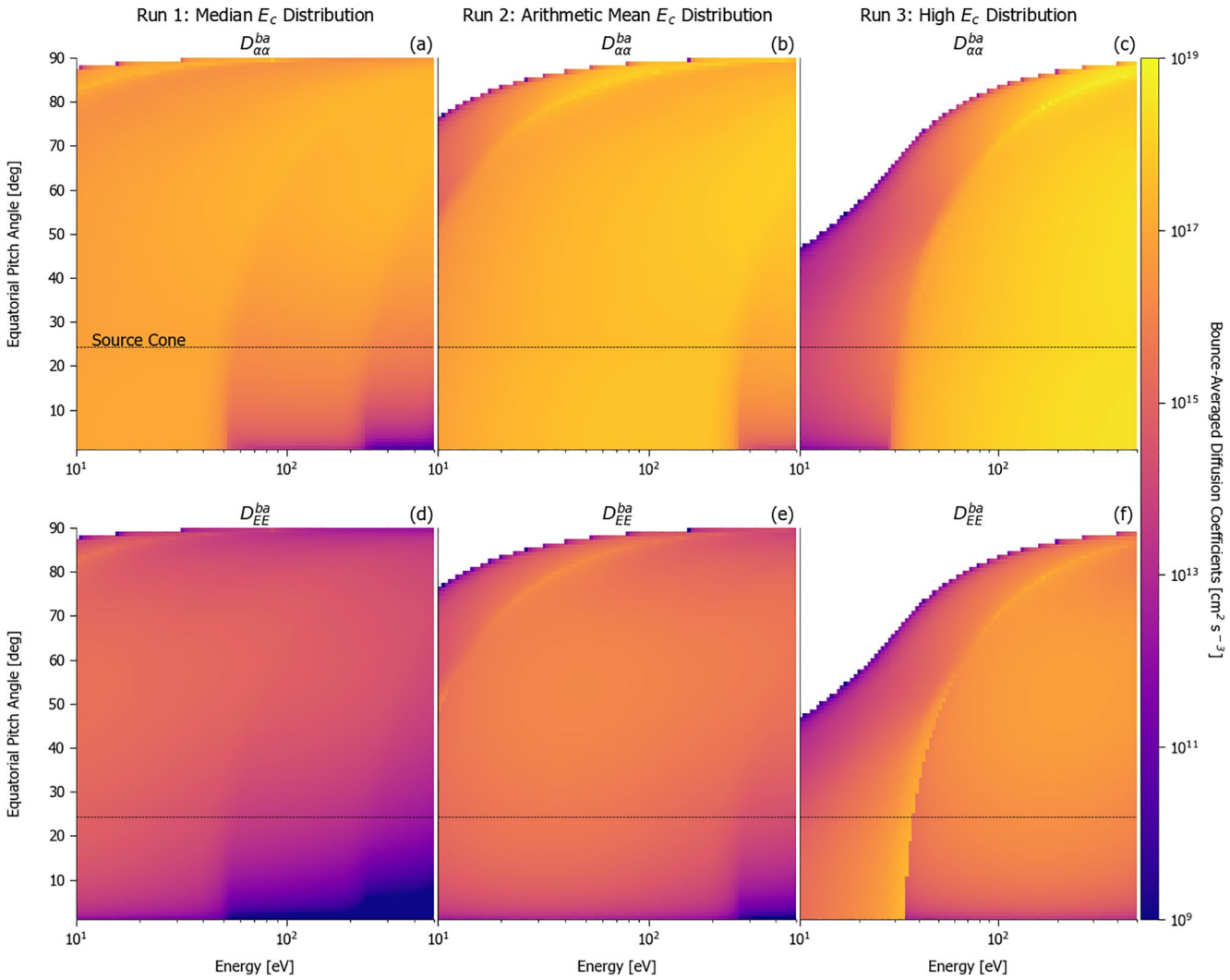

Figure 6. Bounce-averaged pitch angle (a–c) and energy (d–f) diffusion coefficients for Run 1 (a, d), Run 2 (b, e), and Run 3 (c, f). The black dashed line indicates the source cone pitch angle. The color scale is logarithmic and spans 10 orders of magnitude. White regions indicate equatorial plane velocity space regions where the electrons are not in resonance with the imposed waves.

from Run 1 to Run 3. Resonant energy curves can be seen and this comes from the superposition of the harmonics. For the majority of velocity space, the pitch angle diffusion coefficients are greater than the energy diffusion coefficients.

To assess the effectiveness of the wave–particle interaction along the crustal magnetic field, time constants can be estimated via Equation 12 and compared against Coulomb collision time scales. These time constants are shown in Figure 7. The columns from left to right are for Runs 1–3, respectively. The top row plots the pitch angle scattering time scale, the middle row plots the energization time scale, and the bottom row plots the Coulomb collision time scale. The color scale has been chosen such that the color fades to white around 1 h, highlighting the regions of velocity space with fast time scales for each process. MAVEN data show that the high-energy perpendicular peak can be seen by 7 LT, indicating the process responsible happens on subhour time scales. For reference, bounce periods on this crustal field for these energies are between 0.1 and 1.5 s.

Figure 8 compares the multiple time scales of interest against each other. Again, the columns from left to right are for Runs 1–3, respectively, and the black dashed line denotes the source cone pitch angle. Each

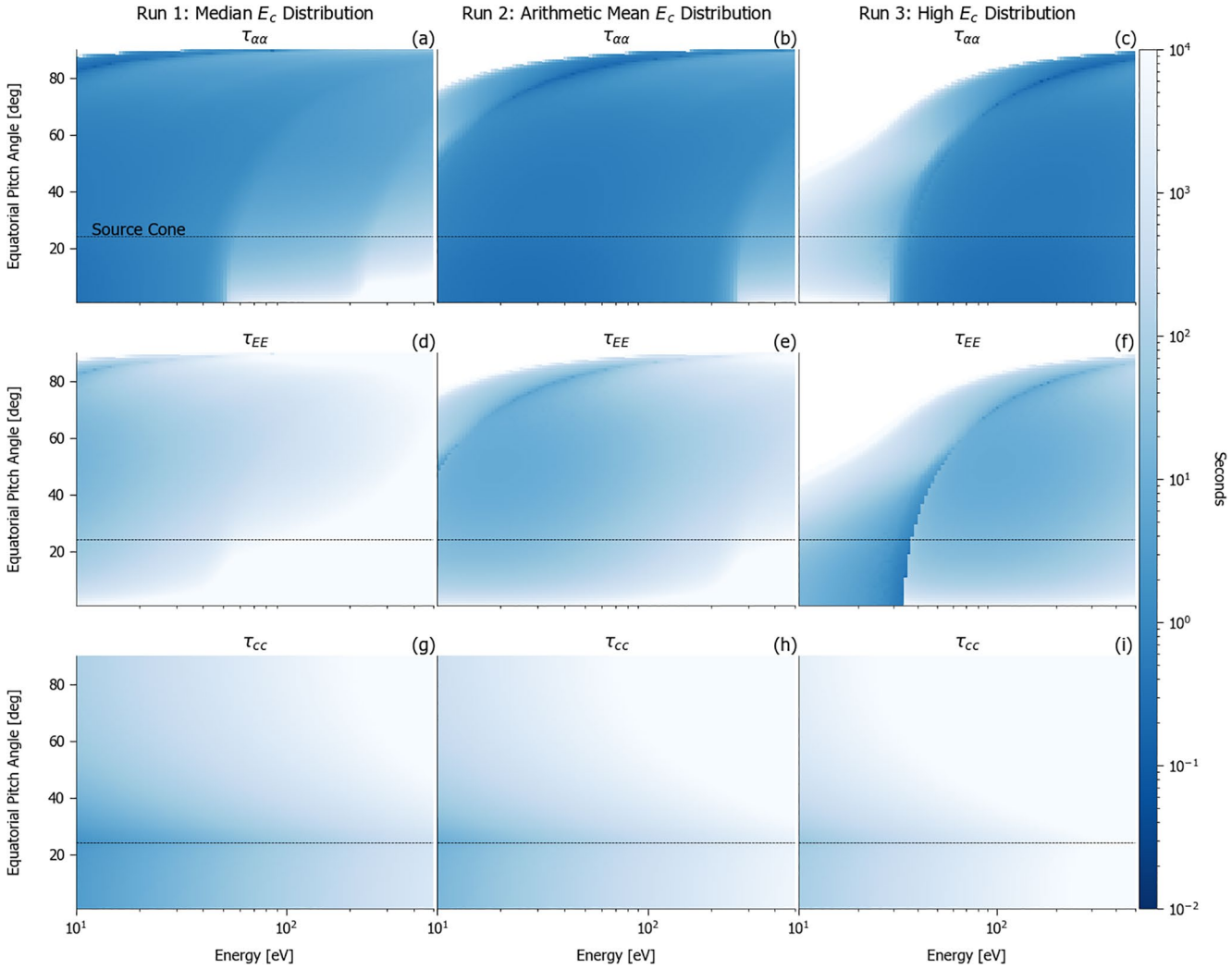

Figure 7. Time constants of interaction for pitch angle scattering (a–c), energization (d–f), and Coulomb collisions (g–i). The columns from left to right are for Runs 1–3, respectively. The color scale is logarithmic and spans 6 orders of magnitude. The black dashed line indicates the source cone pitch angle.

row has a different color bar, but each color bar diverges at a value of 1. The top row plots the ratio of the fastest wave–particle interaction time scale to the bounce period. Blue regions indicate where the wave–particle interaction time scale is subbounce. The middle row plots the ratio of the pitch angle scattering time scale to energization time scale. Blue regions indicate where pitch angle scattering is faster process than energization. Lastly, the bottom row plots the ratio of the fastest wave–particle interaction time scale to the Coulomb collision time scale. Blue regions indicate where wave–particle interactions are faster than Coulomb collision scattering.

Figure 5 shows that electrons with different pitch angles and energies will interact with the prescribed whistler wave at different altitudes. We have used the logarithm base 10 of the diffusion coefficients as weights to quantify the weighted average altitude of wave–particle interactions. Figure 9 shows these results and the columns from left to right are for Runs 1–3, respectively. The strongest interaction between whistler wave and particle occurs near the top of the field line for the trapped electrons. Source cone electrons generally have their strongest interaction at slightly lower altitudes than the trapped electrons but closer to the top of the field line than the exobase altitude.

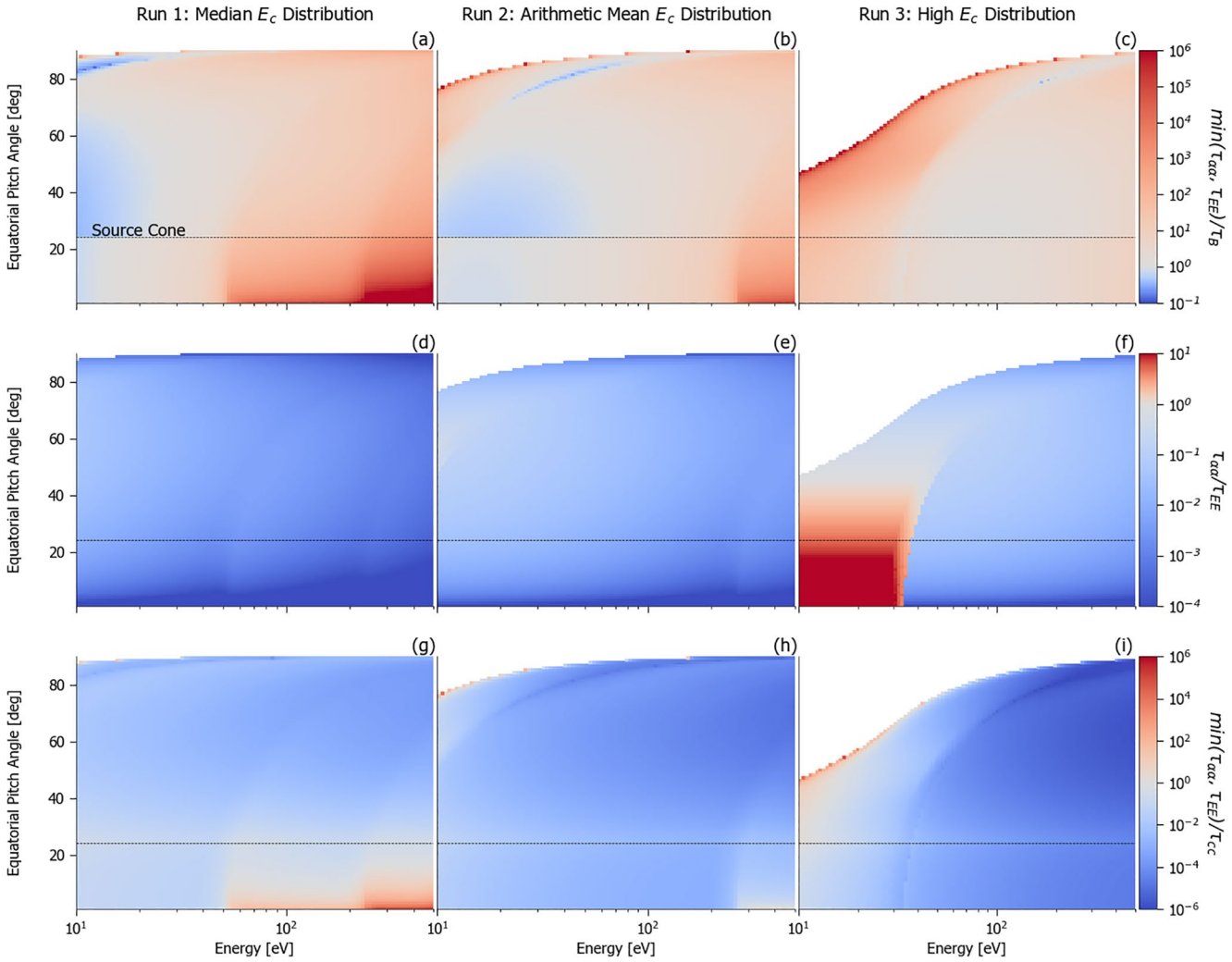

Figure 8. (a–c) Ratio of the fastest wave–particle interaction time scale to the electron bounce period. (d–f) Ratio of the pitch angle scattering time scale to energization time scale. (g–i) Ratio of the fastest wave–particle interaction time scale to the Coulomb collision time scale. The columns from left to right are for Runs 1–3, respectively. The color scales are logarithmic and all diverge at a value of 1. The black dashed line indicates the source cone pitch angle. White regions indicate equatorial plane velocity space regions where the electrons are not in resonance with the imposed waves.

6. Discussion and Conclusions

Several key factors of electron interactions with whistler mode waves have been presented above. We have covered characteristic energies, diffusion coefficients, and order-of-magnitude time constant estimates. We also discussed the limitations of interpreting local wave–particle interactions and modeled bounce-averaged quantities along idealized Martian crustal magnetic fields. Here, we recap those results and interpret them with respect to the relative effectiveness of these waves influencing the velocity space distribution of superthermal electrons on crustal field lines at Mars.

From data taken by the MAG and LPW instruments aboard MAVEN, the characteristic energy of the environment can be calculated. This quantity appears in the equation for the energy of electrons resonant with a particular whistler wave. Determining the typical range of values of this quantity at Mars will help us create idealized altitude profiles to calculate bounce-averaged diffusion coefficients. The majority of magnetic field and plasma density values observed yield characteristic energy values between 0.1 and 100 eV (f_{pe}/f_{ce} = 2,261 and 715), with the peak of the distribution between 1 and 10 eV (f_{pe}/f_{ce} = 715 and 71). The altitude distribution of the characteristic energy shows that at higher altitudes, the characteristic energy is likely to be higher. While for any given crustal magnetic field, the field strength decreases with altitude,

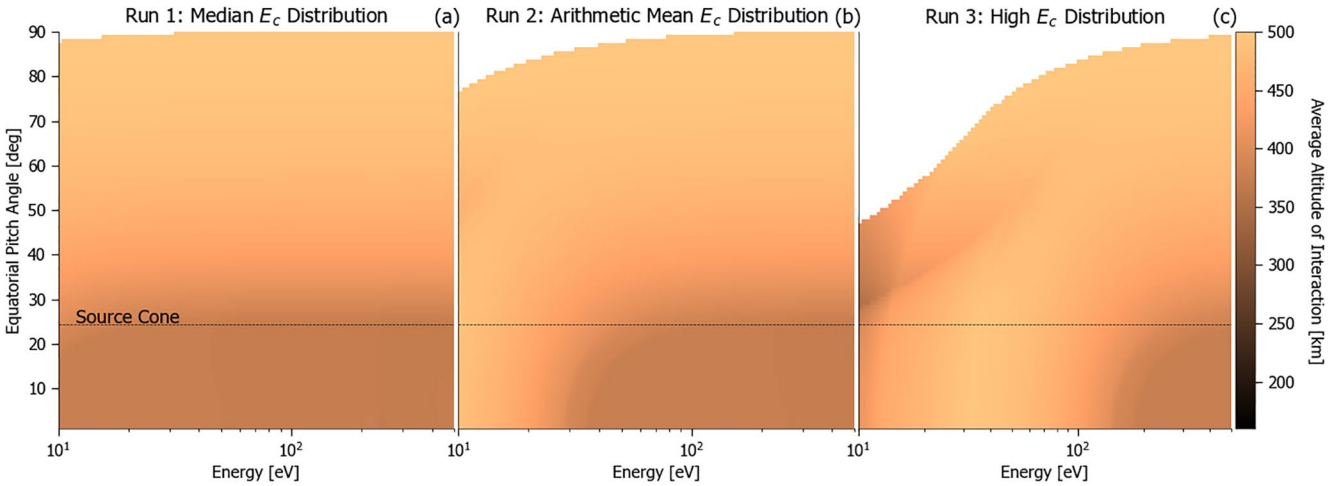

Figure 9. Average altitude of wave–particle interactions weighted by the base 10 logarithm of the local diffusion coefficients. The color scale is linear spanning a range of 350 km. White regions indicate equatorial plane velocity space regions where the electrons are not in resonance with the imposed waves. The black dashed line indicates the source cone pitch angle.

the corresponding decrease to the characteristic energy is likely offset by the orders of magnitude decrease in the electron density. The tail of the characteristic energy distribution gets longer with increasing altitude, indicated by the larger mean-to-median ratios and the spread of the quartiles at higher altitudes. This high-energy tail also exists for vertical magnetic fields. Vertical fields are measured more at low altitudes, where the characteristic energies are lower, so the larger spread in the data is possibly due to low sampling of vertical fields in our data set. There is little-to-no variation in the median characteristic energy as a function of local time. No variations were seen in the electron PADs as a function of local time (Shane et al., 2019), and the little variation in the characteristic energy distribution with respect to local time helps support the hypothesis that wave–particle interactions cause the observed superthermal electron velocity space distribution on Mars crustal field lines.

Our idealized modeling of bounce-averaged diffusion coefficients reveal the complex nature of wave–particle interactions when the particle's trajectory and changing plasma environment is taken into account. We used characteristic energy profiles that match the typical Martian space environment as observed by MAVEN and our wave parameters are based off the observations of Harada et al. (2016) and Fowler et al. (2020). We note again that the wave parameters probably change as the wave propagates along the magnetic field and our assumption that the wave is omnipresent may be false for any given scenario. If whistlers are common on crustal fields, the waves are likely to be of magnetosheath origin, where the temperature anisotropy of the superthermal electrons leads to wave growth (Harada et al., 2016). A ray tracing model can determine if these waves can propagate across draped fields and onto crustal fields. Furthermore, the reflection of these waves could also give insight into where wave–particle interactions are allowed. Whistler waves have been shown to be reflected when the wave frequency approaches the local lower hybrid frequency (e.g., Kuzichev & Shklyar, 2013; X. Xu et al., 2020). Our idealized scenarios had the strongest wave–particle interactions at high altitudes. If there is lower altitude reflection or absorption point, strong wave–particle interactions will still occur.

Runs 1 and 2 have characteristic energy profiles most representative of the average Martian space environment. In both these scenarios, the time scales of the wave–particle interaction are generally greater than a bounce period. Subbounce wave–particle interactions will happen for low-energy electrons (< 20 eV for Run 1 and < 50 eV for Run 2). In both of these regions of velocity space, pitch angle scattering will be a fast process. Once the distribution is sufficiently isotropized, efficient energization can occur. While Shane et al. (2019) did observe source cone distributions for electrons with $E < 60$ eV, the ratio of the field-aligned to perpendicular pitch angles was actually quite low compared to modeling results. The fast time scales of interaction near the source cone boundary allow for the trapped and source cone electron populations to mix while keeping the source cone shape, since there is always a steady source in the dayside ionosphere.

At higher energies, the time scales of wave–particle interaction become much longer than a bounce period and the long time scales at the source cone boundary indicate that the source cone and trapped electron populations are unable to mix sufficiently well, and any change to the trapped electron distribution will have an effect on the PAD. Low-energy electrons pitch angle scattered to perpendicular pitch angles and then energized could have an appreciable effect on the high-energy PAD, especially given the orders of magnitude difference in flux. These two runs imply that wave–particle interactions could produce the observed distributions. In Run 1, the source cone time scales become large compared to a bounce period around 50 eV, near the energy limit where Shane et al. (2019) saw the change from source cone distribution to trapped distribution. The strongest interactions occur at high altitudes, allowing for particles to be trapped more easily. In Run 3, the wave–particle interaction time scales are fairly uniform with respect to energy above 30 eV. The lack of energy dependence does not match with MAVEN observations. In all runs, the wave–particle interactions happen on time scales shorter than Coulomb collisions (except for high-energy source cone electrons in Run 1 and low-energy electrons in Run 3). This occurs even though we change the electron density profile between the three runs, indicating that whistler waves are the dominant process controlling the electron distribution function if present.

The PADs of high-energy electrons observed by both MGS (Brain et al., 2007; Liemohn et al., 2003) and MAVEN (Shane et al., 2019) suggest that unstudied physics are occurring regularly at Mars. In this study, we have investigated the feasibility of whistler waves as the proposed mechanism. The distribution of the characteristic energy on the dayside crustal magnetic fields has been analyzed using MAVEN data. With the average altitude distributions and using the observed wave parameters by Harada et al. (2016) and Fowler et al. (2020), we analyzed the bounce-averaged diffusion coefficients, time scales of the interaction, and altitude at which the strongest wave–particle interaction occurs. The results indicate that wave–particle interactions are more important than Coulomb collisions above the exobase. Runs 1 and 2 showed that the wave–particle interaction process is slow at low energies and allows for mixing between the source cone and trapped population. This could be why the source cone distributions seen at low energies by MAVEN have a low ratio between the parallel and trapped flux. Furthermore, these scenarios had long time scales of interaction at high energies, restricting mixing between the two populations. If there is energization from low to high energies, these electrons are now trapped and this scenario may produce the observed PADs. The flux of electrons at low energies is orders of magnitude larger than the flux at high energies, so only a small fraction of low-energy electrons need to be energized to produce the observed distribution. While time constants can help gauge importance of terms in relation to each other and help determine the efficiency of the process, they cannot give sufficient information about the resulting electron distribution. Modeling of the bounce-averaged quasi-linear diffusion equation is essential for understanding the evolution of electron velocity space distribution due to wave–particle interactions.

Data Availability Statement

All MAVEN data can be accessed through the Planetary Data System (https://pds.nasa.gov/). The filtered pitch angle distribution data set can be found at https://doi.org/10.7302/ya0j-kh60.

Acknowledgments
This work was supported by the National Aeronautics and Space Administration (NASA) grant NNX16AQ04G to the University of Michigan. The MAVEN project is funded by NASA through the Mars Exploration Program.

References

Albert, J. M. (2005). Evaluation of quasi-linear diffusion coefficients for whistler mode waves in a plasma with arbitrary density ratio. *Journal of Geophysical Research*, *110*, A03218. https://doi.org/10.1029/2004JA010844

Andersson, L., Ergun, R. E., Delory, G. T., Eriksson, A., Westfall, J., Reed, H., et al. (2015). The Langmuir Probe and Waves (LPW) instrument for MAVEN. *Space Science Reviews*, *195*(1), 173–198. https://doi.org/10.1007/s11214-015-0194-3

Bougher, S. W., Pawlowski, D., Bell, J. M., Nelli, S., McDunn, T., Murphy, J. R., et al. (2015). Mars global ionosphere–thermosphere model: Solar cycle, seasonal, and diurnal variations of the mars upper atmosphere. *Journal of Geophysical Research: Planets*, *120*, 311–342. https://doi.org/10.1002/2014JE004715

Brain, D. A., Lillis, R. J., Mitchell, D. L., Halekas, J. S., & Lin, R. P. (2007). Electron pitch angle distributions as indicators of magnetic field topology near Mars. *Journal of Geophysical Research*, *112*, A09201. https://doi.org/10.1029/2007JA012435

Connerney, J. E. P., Espley, J., Lawton, P., Murphy, S., Odom, J., Oliversen, R., & Sheppard, D. (2015). The MAVEN magnetic field investigation. *Space Science Reviews*, *195*(1), 257–291. https://doi.org/10.1007/s11214-015-0169-4

Fowler, C. M., Agapitov, O. V., Xu, S., Mitchell, D. L., Andersson, L., Artemyev, A., et al. (2020). Localized heating of the Martian topside ionosphere through the combined effects of magnetic pumping by large-scale magnetosonic waves and pitch angle diffusion by whistler waves. *Geophysical Research Letters*, *47*, e2019GL086408. https://doi.org/10.1029/2019GL086408

Fowler, C. M., Andersson, L., Ergun, R. E., Harada, Y., Hara, T., Collinson, G., et al. (2018). MAVEN observations of solar wind-driven magnetosonic waves heating the Martian dayside ionosphere. *Journal of Geophysical Research: Space Physics*, *123*, 4129–4149. https://doi.org/10.1029/2018JA025208

Glauert, S. A., & Horne, R. B. (2005). Calculation of pitch angle and energy diffusion coefficients with the PADIE code. *Journal of Geophysical Research*, *110*, A04206. https://doi.org/10.1029/2004JA010851

Harada, Y., Andersson, L., Fowler, C. M., Mitchell, D. L., Halekas, J. S., Mazelle, C., et al. (2016). Maven observations of electron-induced whistler mode waves in the Martian magnetosphere. *Journal of Geophysical Research: Space Physics*, *121*, 9717–9731. https://doi.org/10.1002/2016JA023194

Jakosky, B. M., Lin, R. P., Grebowsky, J. M., Luhmann, J. G., Mitchell, D. F., Beutelschies, G., & Zurek, R. (2015). The Mars Atmosphere and Volatile Evolution (MAVEN) mission. *Space Science Reviews*, *195*(1), 3–48. https://doi.org/10.1007/s11214-015-0139-x

Jordanova, V. K., Kozyra, J. U., & Nagy, A. F. (1996). Effects of heavy ions on the quasi-linear diffusion coefficients from resonant interactions with electromagnetic ion cyclotron waves. *Journal of Geophysical Research*, *101*(A9), 19771–19778. https://doi.org/10.1029/96JA01641

Kennel, C. F., & Engelmann, F. (1966). Velocity space diffusion from weak plasma turbulence in a magnetic field. *Physics of Fluids*, *9*(12), 2377–2388. https://doi.org/10.1063/1.1761629

Kuzichev, I. V., & Shklyar, D. R. (2013). Full-wave description of the lower hybrid reflection of whistler waves. *Plasma Physics Reports*, *39*(10), 795–808. https://doi.org/10.1134/S1063780X13090043

Liemohn, M. W., Khazanov, G. V., & Kozyra, J. U. (1997). Guided plasmaspheric hiss interactions with superthermal electrons: 1. Resonance curves and timescales. *Journal of Geophysical Research*, *102*(6), 11619–11623. https://doi.org/10.1029/97JA00825

Liemohn, M. W., Mitchell, D. L., Nagy, A. F., Fox, J. L., Reimer, T. W., & Ma, Y. (2003). Comparisons of electron fluxes measured in the crustal fields at Mars by the MGS magnetometer/electron reflectometer instrument with a *B* field-dependent transport code. *Journal of Geophysical Research*, *108*(E12), 5134. https://doi.org/10.1029/2003JE002158

Lyons, L. R. (1974a). General relations for resonant particle diffusion in pitch angle and energy. *Journal of Plasma Physics*, *12*(1), 45–49. https://doi.org/10.1017/S0022377800024910

Lyons, L. R. (1974b). Pitch angle and energy diffusion coefficients from resonant interactions with ion–cyclotron and whistler waves. *Journal of Plasma Physics*, *12*(3), 417–432. https://doi.org/10.1017/S002237780002537X

Lyons, L. R., Thorne, R. M., & Kennel, C. F. (1972). Pitch-angle diffusion of radiation belt electrons within the plasmasphere. *Journal of Geophysical Research*, *77*(19), 3455–3474. https://doi.org/10.1029/JA077i019p03455

Shane, A., Liemohn, M., Florie, C., & Xu, S. (2019). Misbehaving high-energy electrons: Evidence in support of ubiquitous wave–particle interactions on dayside Martian closed crustal magnetic fields. *Geophysical Research Letters*, *46*, 11689–11697. https://doi.org/10.1029/2019GL084919

Xu, S., Liemohn, M., Bougher, S., & Mitchell, D. (2016). Martian high-altitude photoelectrons independent of solar zenith angle. *Journal of Geophysical Research: Space Physics*, *121*, 3767–3780. https://doi.org/10.1002/2015JA022149

Xu, S., Mitchell, D., Liemohn, M., Fang, X., Ma, Y., Luhmann, J., & Jakosky, B. (2017). Martian low-altitude magnetic topology deduced from MAVEN/SWEA observations. *Journal of Geophysical Research: Space Physics*, *122*, 1831–1852. https://doi.org/10.1002/2016JA023467

Xu, X., Chen, L., Zhou, C., Liu, X., Xia, Z., Simpson, J. J., & Zhang, Y. (2020). Two-dimensional full-wave simulation of whistler mode wave propagation near the local lower hybrid resonance frequency in a dipole field. *Journal of Geophysical Research: Space Physics*, *125*, e2019JA027750. https://doi.org/10.1029/2019JA027750

Zhao, L., Yu, Y., Delzanno, G. L., & Jordanova, V. K. (2015). Bounce- and MLT-averaged diffusion coefficients in a physics-based magnetic field geometry obtained from RAM-SCB for the 17 March 2013 storm. *Journal of Geophysical Research: Space Physics*, *120*, 2616–2630. https://doi.org/10.1002/2014JA020858